Dual-pulse generation from a velvet cathode with a new inductive voltage adder for x-ray flash radiography applications

R. Delaunay,[1] B. Cadilhon,[2] L. Courtois,[2] I. Mousseau,[2] J. M. Plewa,[3] C. M. Alvinerie,[1] B. Cassany,[2] C. Vermare,[2] T. D'Almeida,[1] M. Ribière,[1] and R. Maisonny[1,*]

[1]*CEA, DAM, GRAMAT, F-46500 Gramat, France*
[2]*CEA, DAM, CESTA, F-33114 Le Barp, France*
[3]*TRAD Tests and Radiations, 907 L'Occitane, 31670 Labège Cedex, France*

(Received 8 October 2021; accepted 19 April 2022; published 15 June 2022)

The evolution of two intense pulsed electron beams for an x-ray flash radiography application is characterized in a coupling of experimental and simulation studies. For this purpose, experiments were performed at Commissariat à l'Energie Atomique et aux Energies Alternatives with a new dual-pulse inductive voltage adder named "Mi2." This experimental setup has been designed and built to produce two intense pulsed electron beams of 2 kA, 700 keV, and 80 ns full width at half maximum from a velvet cold cathode. The delay between the pulses ranges from tens of nanoseconds to a few microseconds. This study quantifies the effect of the plasma dynamics on the beam current of the second pulse, which represents an important parameter from the beam transport point of view. A multidimensional particle-in-cell simulation model is used to provide a numerical analysis in order to determine the influence of velvet plasma dynamics on the second pulse. Analysis of the experimental results indicates that the motion of the electron extraction zone within the expanding plasma remains lower than 1 mm for 3 μs delay, inducing a minor impact on the beam current extracted from the velvet cathode. Based on the developed model, this plasma expansion induces an increase of 5% for the current extracted from the second pulse with a delay of 1 μs for two pulses having the same voltage, which is consistent with linear induction accelerator injector parameters for multiple pulse use.

DOI: 10.1103/PhysRevAccelBeams.25.060401

I. INTRODUCTION

X-ray flash radiography is a powerful diagnostic used worldwide [1–6] for investigating the structural response of matter under impulsive loading during hydrodynamic experiments. Recently, significant efforts were undertaken in order to develop and optimize multipulse radiographic facilities [7–11]. Radiographic sources based on the linear induction accelerator (LIA) have successfully demonstrated multipulse radiography capabilities, notably, DARHT-II [9] and DRAGON-II [10]. In order to achieve this multiframe measurement, different architectures may be used.

The first one is the production of a long and intense electron beam chopped with a kicker system at the end of the LIA. The kicker system slices the beam before the x-ray conversion target, hence producing the multipulse x-ray source. This is the architecture of DARHT-II, where a long beam of 1.7 kA and 1.7 μs flattop is produced by a hot dispenser cathode and accelerated at 17 MeV before being sliced up into four pulses [9]. Although this is reliable, the size of the accelerator remains large due to the size of the magnetic core in the induction cell needed to accelerate the beam during its entire duration.

Another architecture leads to the production of multipulse electron beams directly at the injector. This is an interesting alternative, because it minimizes the volume of magnetic materials needed and reduces the cost of the accelerator and its size. DRAGON-II [10] is based on this concept, where three pulses of 60 ns at 17 MeV with 2 kA for each pulse are produced from a thermionic cathode. However, the thermionic cathode requires a very efficient vacuum system to reach a pressure on the order of 10^{-6} Pa. This high vacuum requirement leads to a complex injector design of the accelerator and is not easily compatible with ferrite under a vacuum induction cell such as those of the Expériences de Physique Utilisant la Radiographie Eclair (EPURE) axis-1 LIA [2]. In the injector, a velvet cathode may also be a good option for producing two or more pulses [10,12–14]. However, several studies, mainly done for high-power microwave applications at a repetition rate of 1–100 Hz, have shown that velvet plasma has a

*remi.maisonny@cea.fr

dynamics which affects the properties of the electron beam extracted from the cathode [15–19].

For flash radiography application, and especially from a beam dynamics point of view, the beam properties significantly affect the beam transport and, hence, the x-ray performance. Xia and collaborators have observed in multiple pulse mode a variation of the beam properties due to cathode plasma motion [15,20–22]. Those studies are supported by a previous work with velvet cathodes realized in 1996 on the Advanced Test Accelerator injector used in dual-pulse experiments at a voltage of 1 MV and a current of approximatively 2.5 kA [12].

The present study aims to quantify how the second pulse is affected by the plasma dynamics when it is produced with a delay comprised between tens of nanoseconds and a few microseconds after the first pulse. The results provided by this study are required to perform multiple beam transport using a velvet cathode as a function of the delay between the pulses and to predict the radiographic performance of each pulse.

For this purpose, a dedicated inductive voltage adder (IVA), named Mi2, has been built at Commissariat à l'Energie Atomique (CEA). This new high pulsed power setup allows the production of two intense pulsed electron beams from a velvet cathode. The pulse parameters are typically 700 keV, 2 kA, and 80 ns FWHM with a variable delay between the pulses. Particle-in-cell (PIC) simulations were employed to analyze and infer the plasma dynamics from the experimental results obtained with Mi2. First, Sec. II provides an overview of the experimental setup dedicated to the production of the two pulses. Section III describes the simulation conditions of the PIC model. Then Secs. IV and V present the analysis of the experimental results and the evolution of the electron extraction zone correlated to plasma dynamics as a function of the time delay between the two pulses. Finally, conclusions and perspectives of this dual-pulse IVA and this numerical approach are drawn.

II. EXPERIMENTAL SETUP

Mi2 was designed and built as a test bed induction injector in the framework of a future multipulse electron LIA for flash radiography. It succeeds previous works carried out on the dual-pulse linear transformer driver cavity [23]. This IVA is composed of a dual-pulse driver and four induction cells [Fig. 1(a)]. Two 700 kV pulses are applied across the diode gap in order to produce two 2 kA

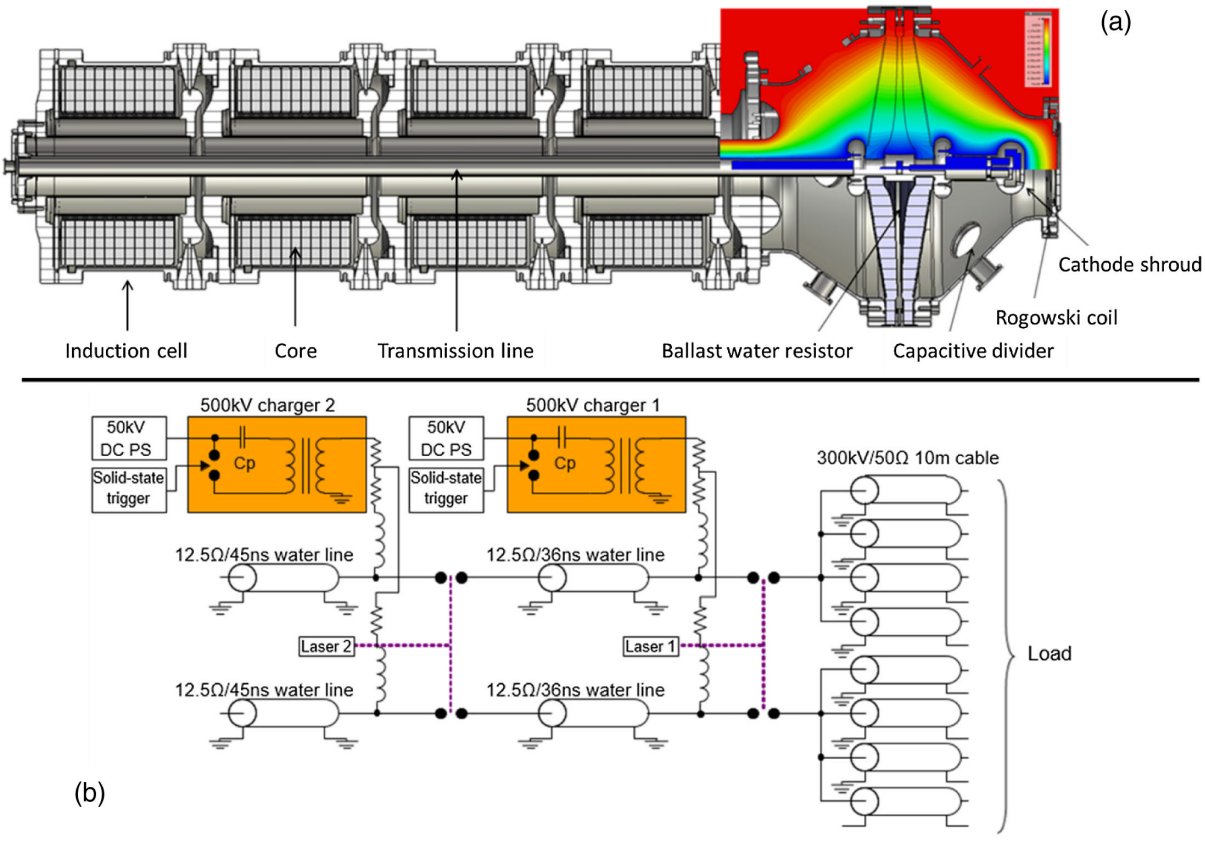

FIG. 1. (a) Cut view of the Mi2 IVA including four ferrite induction cells, ballast radial resistor, and vacuum diode enclosure. Electrostatic potential distribution in the diode region [24] (right part of the figure). (b) 250 kV dual-pulse driver based on laser-triggered series water pulse forming lines.

electron pulse from a velvet cold cathode. The delay between the two pulses can be adjusted from tens of nanoseconds up to few microseconds.

A. Dual-pulse driver

The injector driver is a laser-triggered series of water pulse forming lines (PFLs) able to produce two 250 kV square pulses with high shot-to-shot reproducibility. The design and the work performed on the driver are described in a previous paper [25]. The pulses are generated by the discharge of 500 kV and 12.5 Ω water PFLs in series. The two air-pressurized spark-gap switches are triggered by a common 80 mJ/8 ns 266 nm Nd:YAG laser and a set of UV optics. This reduces the jitter of the switches to the nanosecond range. By varying the time delay between the two laser triggerings, the time delay between the two pulses can be adjusted from some tens of nanoseconds to a few microseconds. The diagram in Fig. 1(b) is a simplified electrical schematic of the generator. The two dual water lines are charged in 3 μs at around 500 kV (27 kA current pulse from the 1200 nF primary capacitors) by two common transformer-based pulsed chargers through L-R circuits. The energy is transported to the four induction cells by eight 10 m 300 kV 50 Ω cables, two cables for each cell.

Typical voltage pulses are presented in Fig. 2. These waveforms correspond to five delays between pulses, from 80 ns to 2 μs. The second pulse PFL is slightly longer than the first one. The ripples coming from mismatches between generator, cables, and load caused by the first pulse also affect this second voltage plateau.

B. IVA design

The IVA is based on four ferrite induction cells coming from the accelerating section of the former LIA prototype of the EPURE axis-1 accelerator [26] coupled to a vacuum diode. Each cell includes 11.5 CEA-made ferrite torus (outer diameter, 500 mm; inner diameter, 250 mm; 20 mm thick) under vacuum serving as a 1:1 isolating transformer so that each individual dual line of the dual-pulse driver can be grounded in the voltage summing process [Fig. 1(a)]. The 50-mm-diameter stalk and the overall cellblock housing are made of stainless steel. Each cell has four ports; the top and bottom ones are connected to the vacuum pumping system. Ports on both sides are connected to the dual-pulse driver via two comp cans containing adjustable ballast resistors to match the generator impedance to the IVA impedance. An 800 A peak current pulse from a reset pulser premagnetizes the ferrite torus to the opposite maximum induction before the dual high-voltage shot. One of the two comp cans of a cell is equipped with a 100 μH decoupling inductor to connect the reset pulser and to protect it against the main high-voltage pulses.

The highest electric field region is the fourth gap section. So maximum voltage is deliberately limited to 800 kV, which corresponds to 200 kV for the dual-pulse generator. Hence, the electric field is limited to a value lower than 300 kV/cm to mitigate the risk of flashover and to prevent field emission processes.

Mi2 is equipped with electrical diagnostics. The gap voltage is measured on each cell using capacitive divider in

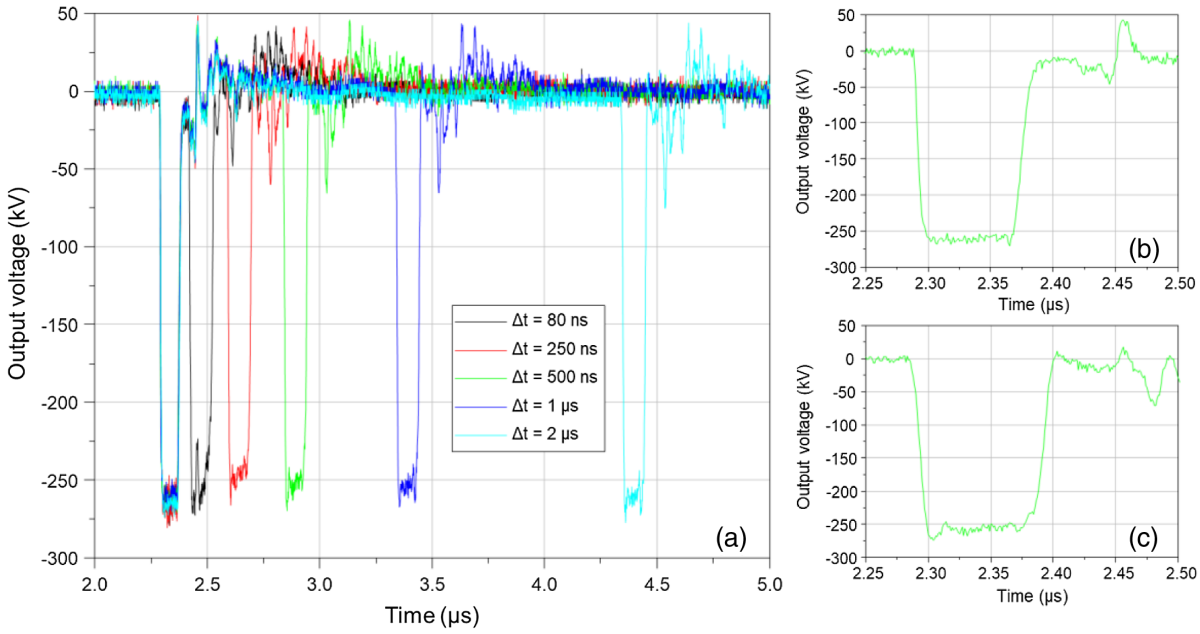

FIG. 2. (a) Output voltage on a resistive matched load at nominal charging voltage for different time delays Δt between the two pulses. (b) Output voltage of the first pulse with $\Delta t = 500$ ns. (c) Output voltage of the second pulse with $\Delta t = 500$ ns. The second pulse is time shifted.

comp cans. The total IVA current (secondary side of the transformer) and the current from each driver (primary sides of the transformer) is measured using Rogowski coils. The diode voltage is also recorded from a capacitive divider.

The diode chamber, illustrated in Fig. 1(a), includes a $CuSO_4$ liquid ballast resistor to match the diode impedance and a stainless steel shroud to hold the cathode in place and shape the electric field. The cathode consists of a disk of velvet stretched on a metal plate. The anode is made of a thin Mylar-aluminized sheet. Potential lines, from 0 to −700 kV, are plotted from an electroquasistatic calculation taking into account the finite conductivity of the ballast resistor mixture.

In LIAs, beams are usually produced at the injector with energy of several MeV, which is not the case in this test bed injector. Nevertheless, the plasma dynamics are believed to be driven by the current density, the electric field, and the temperature [15,18]. The anode-cathode distance and the cathode radius are adjusted to match the electric field and current density of a LIA. Furthermore, the time length of Mi2 pulses is representative of an accelerator. The following section describes the numerical approach used to characterize the pulses.

III. NUMERICAL MODELING

Electron beams are produced by a 5-cm-diameter velvet cathode inside the Mi2 injector, which delivers high-voltage pulses of 700 kV across a diode gap of 3.5 cm. The application of a strong electric field results in plasma formation on the cathode surface due to a surface flashover when the field exceeds a threshold of a few tens of kV/cm [16]. Then the electrical field extracts a space-charge-limited (SCL) electron flow from the plasma. Based on the Child-Langmuir law [27,28], the SCL current density J for a 1D planar diode with the anode-cathode distance d_{AK} in centimeters and the voltage V in volts (in the steady-state nonrelativistic regime) is given by

$$J = \frac{4\varepsilon_0}{9}\sqrt{\frac{2e}{m_e}}\frac{V^{3/2}}{d_{\mathrm{AK}}^2}.$$

By considering that the current density is uniform for an emitting surface with a radius r_c in a cylindrical diode geometry, the following relationship is obtained:

$$I = \frac{4\varepsilon_0}{9}\sqrt{\frac{2e}{m_e}}\left(\frac{\pi r_c^2}{d_{\mathrm{AK}}^2}\right)V^{3/2}.$$

This equation links the extracted current I, for a given extraction voltage V, with the diode geometry, i.e., the surface πr_c^2 and the gap distance d_{AK}. The quantity $\frac{I}{V^{3/2}}$ corresponding to the gun perveance P depends only on the diode geometry and the particle type. Consequently, the gun perveance value remains constant during the operation of the diode as long as there is no modification in its geometry, assuming that no bipolar flow occurs in the diode from the electron interaction with the anode [17]. Otherwise, bipolar flow can alter the diode performance significantly [29]. On the opposite, a modification of the gun perveance indicates a change in the diode geometry. The analysis of plasma influence in velvet cathodes relies on this principle. The difficulty consists in establishing the most accurate law in order to connect I, V, and the geometry of the diode. In their work on explosive emission with velvet cathodes, Coleman and co-workers found the best agreement for calculated values to fit the experimental data for an exponent value of 1.3473 for the voltage V [19]. Based on the analytical model of Lau [30], Krasik and co-workers proposed a more complex analysis of the electron beam produced by velvet cathodes considering two-dimensional effects [18]. Despite those studies, analytical laws are not sufficient to take into account the reduction of edge effects in explosive emission diodes when the latter are recessed [31]. Multidimensional simulation codes offer a more accurate modeling to study the physics of SCL flow that takes place within complex geometries. The present model based on PIC simulation includes many effects (geometry, relativistic regime, variation of the current density, influence of the anode, etc.) and links the current I with the voltage V for a given geometry of the diode. A good agreement between simulation and experiment was obtained with this method for the single pulse produced with the EPURE axis-1 injector [2]. This work proposes to extend this numerical model to dual-pulse experiments to infer the plasma dynamics from experimental data in order to study the influence of velvet plasma dynamics on the extracted current for the second pulse.

A PIC simulation model has been developed with the fully relativistic 3D large scale plasma (LSP) code [32] to predict beam dynamics for the two pulses of the Mi2 injector. Particles are pushed in the simulation with a semi-implicit particle field solver. The time step is 0.6 ps approximatively. Figure 3 shows an example of the simulation geometry used to perform the numerical study. Simulations are achieved in a 2D cylindrical geometry (r,z) with a radius of the velvet emissive surface $r_c = 2.5$ cm, an anode-cathode distance $d_{\mathrm{AK}} = 3.5$ cm, and mesh dimensions of 0.025 cm. The recess value ranges from 0 to 5 mm to study the evolution of the cathode current with the initial position of the extracted electron beam. The recess corresponds to the depth of the emission surface. SCL electron emission is used in simulations to model the current extracted from the velvet cathode. Electron emission from the velvet cathode is supposed to be uniform and is allowed when the electric field exceeds 20 kV/cm [33]. A mean electron energy of 3.5 eV is used in the simulation based on a complex 0D collisional radiative model experimentally validated with a velvet cold cathode used in EPURE

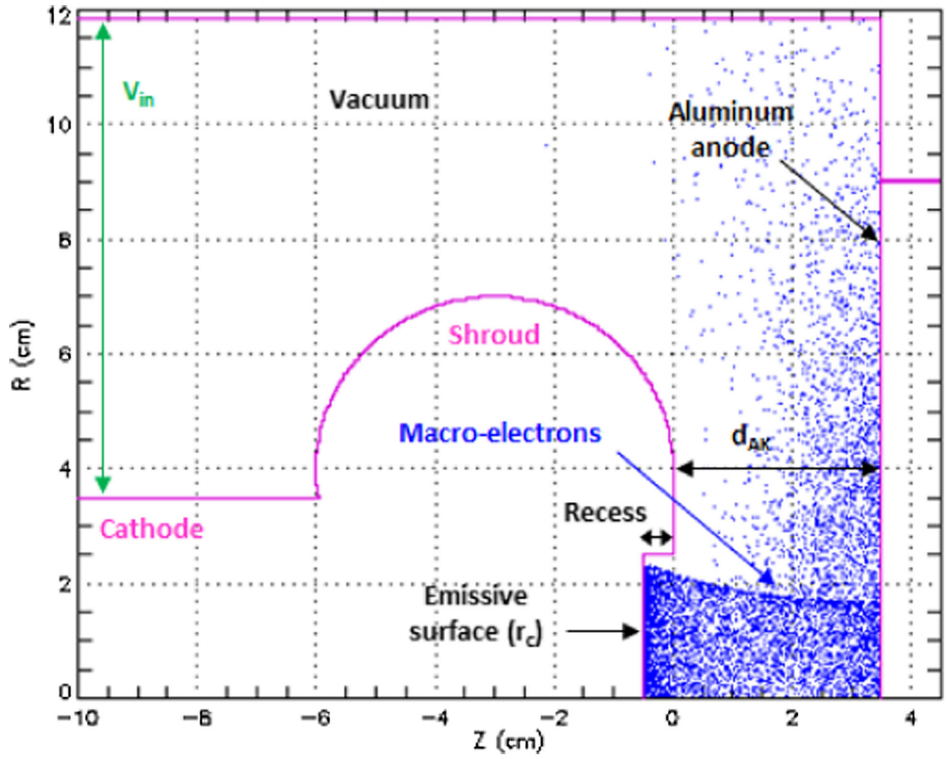

FIG. 3. Mi2 diode geometry used in the simulation with a 2.5 cm cathode radius, an anode-cathode gap of 3.5 cm, and a recess of 5 mm.

axis-1 [34]. Proton emission at the aluminum anode is modeled by a Monte Carlo treatment with the integrated tiger series code [35] for temperatures exceeding 400 °C [36].

IV. COMPARISON WITH EXPERIMENTAL RESULTS

The left panel in Fig. 4 presents a typical experimental voltage for V_{in} (black curve) and the voltage used to perform the simulation (blue curve) for a delay $\Delta t = 2$ μs between the two pulses. The voltage implemented in the simulation reproduces well the amplitude and time profiles of experimental data.

The right panel in Fig. 4 compares the diode extracted current from the simulation (blue curve) and the current measured experimentally (black curve). As mentioned previously, the diode geometry, i.e., emission conditions, is identical for both pulses. At the first radiography axis of EPURE, it has been shown that the emission surface is slightly downstream of the velvet surface on the order of

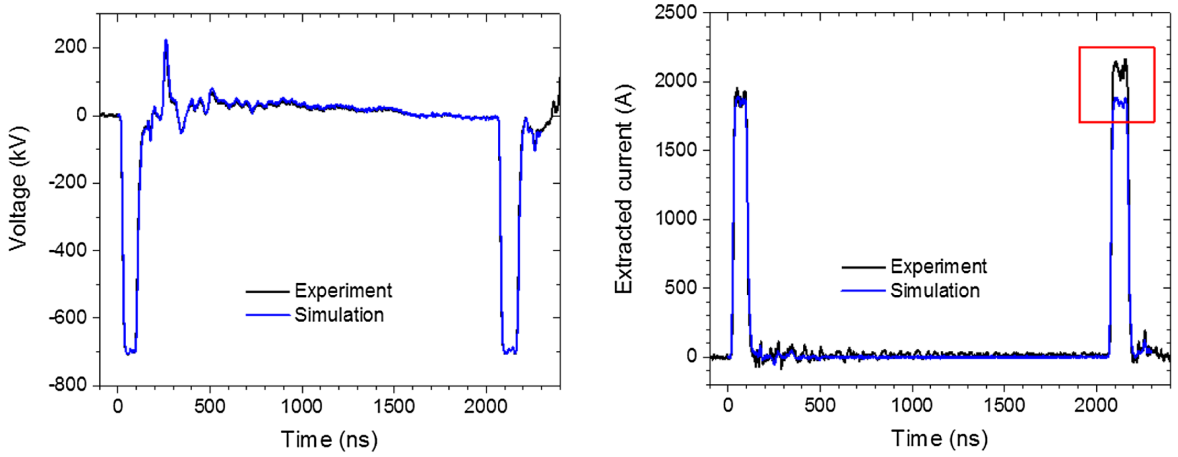

FIG. 4. Left: diode voltage V_{in} used in the simulation (blue curve) and measured experimentally (black curve) for a delay of 2 μs between the two pulses. Right: extracted current measured experimentally (in black) and simulated (in blue) for a delay of 2 μs.

1 mm due to the thickness of the plasma sheath [2]. This difference induces an uncertainty to accurately model the diode geometry. That same difference between the velvet position and the emission surface is observed in Mi2, where the velvet position for this experiment is estimated at a recess of 2.3 mm. It is necessary to take into account this space shift in order to properly reproduce the extracted current of the first pulse. The emission surface used in the simulation is recessed 1.75 mm to match the extracted current I_{ext} of the first pulse.

A very good agreement on I_{ext} is obtained between simulation and experiment for the first pulse with an emission surface recessed 1.75 mm. But, however, it is interesting to observe that this is not the case for the second pulse (see the red square in Fig. 4) for which the measured current is 250 A higher than the simulated current.

Experimentally, this current discrepancy may be associated to different mechanisms affecting the diode operation: a voltage increase, an ion flow coming from the anode, and a modification of the diode geometry induced by the velvet plasma expanding in the gap between the first and the second pulse. The simulation already includes the voltage evolution as a function of the time, and, in addition, the voltage difference between the two pulses is minimal for this experiment excluding the effect of a voltage increase. The temperature rise induced at the anode surface by electron energy deposition has been calculated in order to investigate the impact of an ion flow coming from the anode. The results of the simulation show that the temperature remains lower than 400 °C, which is the temperature usually considered to produce an anode plasma formation [36]. Thus, an ion flow coming from the anode is also excluded. The last assumption considers that the geometry of the diode varies between the first and second pulses. This result is the consequence of velvet plasma expansion at the cathode surface. Currently, the diode geometry remains unchanged during the time of the simulation. Additional simulations have been made with different recess values (see Fig. 5) mimicking an emission surface shift between the pulses.

Figure 5 shows the time evolution of the current for different recesses from 0 to 5 mm studied by simulations. Figure 5 highlights that the extracted current is strongly related to the recess value, i.e., to the emission surface. The extracted current increases when the recess decreases. This current evolution is the consequence of the electric field decrease at the cathode surface with a larger recess. This result has already been observed experimentally on EPURE axis-1 [2] and is in good agreement with the numerical studies made on DARHT-I [37] and SCORPIUS [38].

The simulation model developed for this study establishes a relationship between the diode current and the diode voltage as a function of time, neglecting the effect of plasma expansion in the diode. The right panel in Fig. 5 presents the evolution of the current with the recess for the first pulse at $t = 60$ ns (black square) and the second pulse at $t = 2120$ ns (red circle). For both pulses, neither plasma expanse nor modifications in the diode configuration are taken into account in the numerical model. As the plasma effect is not modeled in the simulation for the second pulse, the difference between experiments and simulations allows the quantification of this effect.

A third-order polynomial fit is made for each pulse represented by a dotted line in Fig. 5 (right). For the first pulse, at $t = 60$ ns, the polynomial which links the extracted current I_{ext} (in A) and the recess r (in millimeters) is $I_{ext} = 2681.33 - 591.22\,r + 90.61\,r^2 - 6.91\,r^3$ and for the second pulse, at $t = 2120$ ns, $I_{ext} = 2620.60 - 582.77\,r + 90.65\,r^2 - 7.02\,r^3$. Fits are very similar in this simulation case, because the voltages during the two pulses are almost identical (less than 15 kV difference). This method is applied for each configuration of the simulation to link the current measured

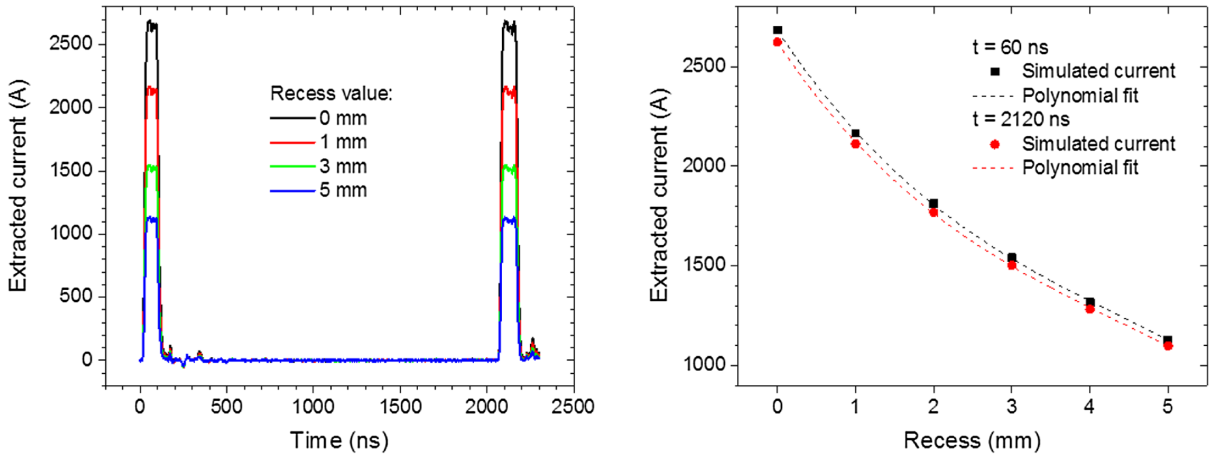

FIG. 5. Left: evolution of the extracted current for different recess values from 0 to 5 mm used in the simulation with a delay of 2 μs between the two pulses. Right: evolution of the extracted current as a function of the recess value for the first pulse at $t = 60$ ns (black square) and the second pulse at $t = 2120$ ns (red circle). The dotted lines correspond to third-order polynomial fits.

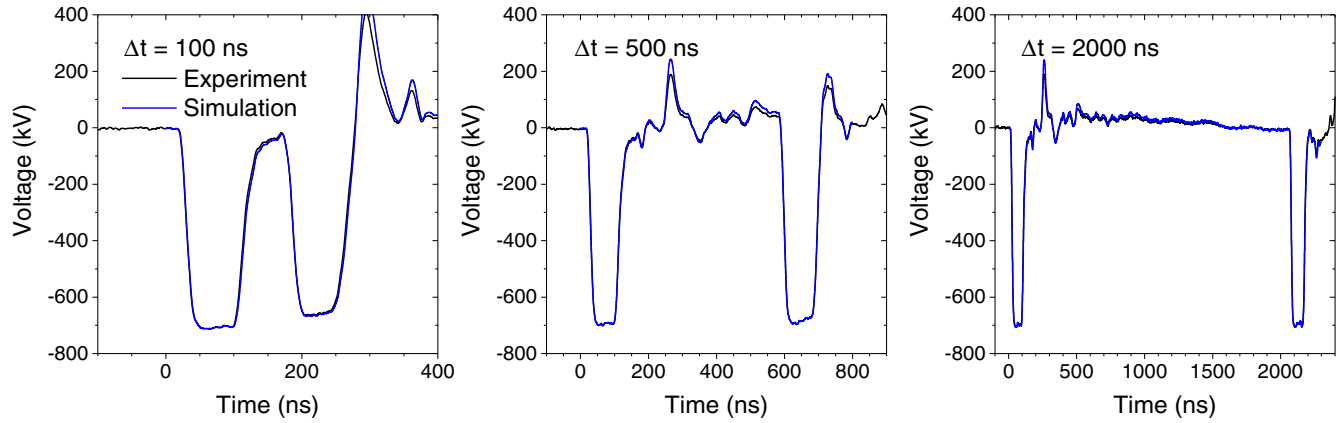

FIG. 6. Comparison of simulated (blue curve) and experimental voltages (black curve) for Δt ranging from 100 to 2000 ns.

experimentally with the recess position in order to follow the evolution of the electron emission surface as a function of the delay. The method proposed here to deduce the relative evolution of the emission surface consists in finding the recess required to produce the same extracted current from the second pulse by simulation and experimentally. The fits realized in Fig. 5 allow deducing in this particular case that the emission surface is shifted approximatively 0.7 mm in the gap toward the anode between the two pulses. This leads to about a 300 A shift after a 2 μs delay.

V. EVOLUTION OF THE PLASMA EXPANSION WITH Δt

A set of experiments was performed at a diode voltage of 700 kV with different delays Δt ranging from 100 to 2000 ns and a velvet surface position estimated at a recess of 2.3 mm. A comparison for each Δt of the simulated and experimental voltages is presented in Fig. 6. As previously mentioned, voltages used in simulations (blue curves) are in very good agreement with the experimental voltages (black curve). It is important to notice that the voltage of the second pulse depends on Δt. This comes from voltage reversal between the two pulses due to the design of the injector and its transmission line. This phenomenon implies the necessity to realize a specific simulation for each Δt.

A comparison of simulated and experimental extracted currents I_{ext} as a function of Δt is presented in Fig. 7. The red and blue curves represent simulated currents for a recess of 1 and 2 mm, respectively. The black curve corresponds to the current measured experimentally, showing that, despite the fact that the experimental signal is slightly noisy, the reproducibility shot to shot of the first pulse is good. For all Δt, I_{ext} of the first pulse is close to the simulation case with a recess of 2 mm (blue curve in Fig. 7).

Figure 7 highlights that I_{ext} of the second pulse changes with Δt. The experimental current (black curve) is initially close to the simulated current for a recess of 2 mm (blue curve) for the second pulse with $\Delta t = 100$ ns but approaches the simulated current for a recess of 1 mm (red curve) when Δt increases. For $\Delta t = 2000$ ns, the experimental current measured for the second pulse matches the simulated current for a recess of 1 mm pretty

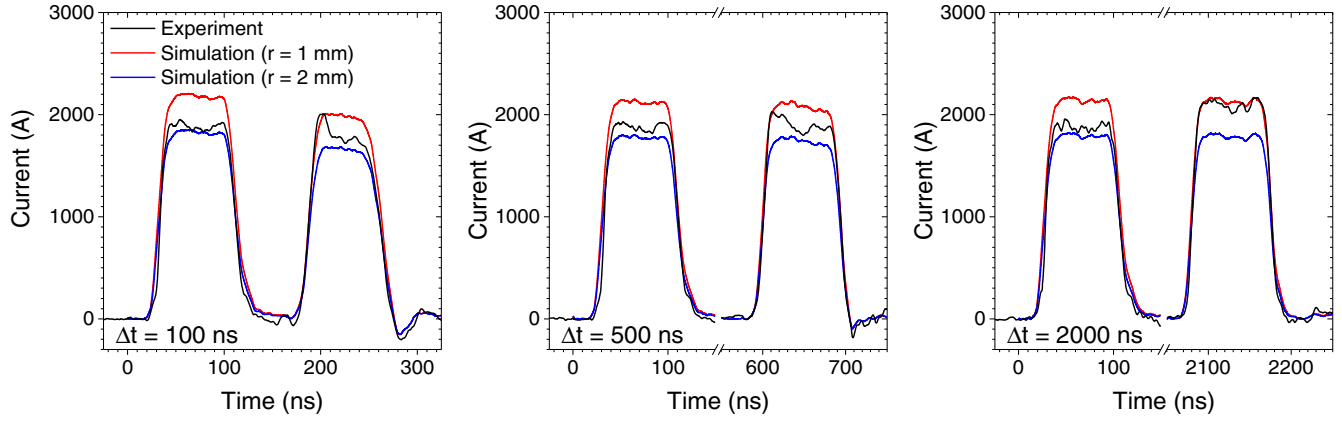

FIG. 7. Comparison of simulated and experimental extracted currents for different Δt. Red and blue curves represent simulated current for a recess r of 1 and 2 mm, respectively. Black curves correspond to experimental measurements of the extracted current. Note that the timescales are different.

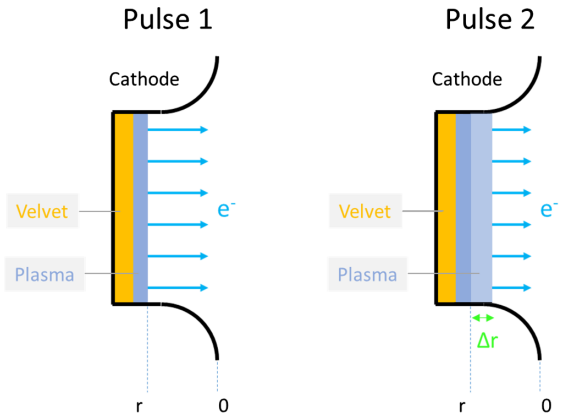

FIG. 8. Schemes of the evolution of the plasma boundary for the first pulse (left part of the figure) and for the second pulse (right part of the figure). Δr corresponds to the difference between the recess at the first and at the second pulse.

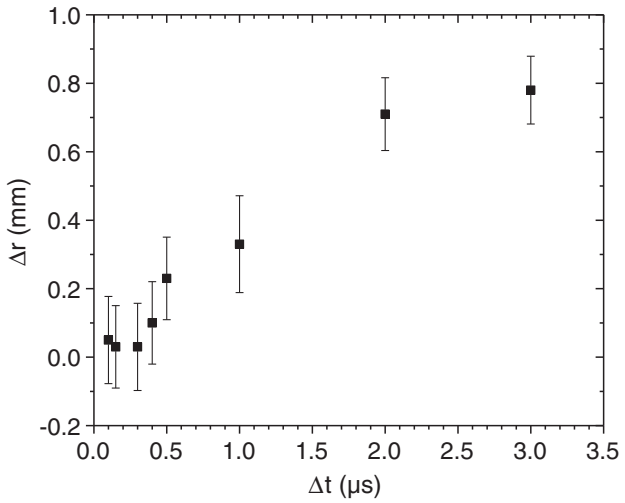

FIG. 9. Evolution of Δr with Δt ranging from 100 ns to 3 μs.

well. As experimental data (black curve) are slightly noisy, it is complicated to measure plasma dynamics during the pulses. The beginning of the second pulse for $\Delta t = 100$ ns presents a behavior close to the simulation with a recess of 1 mm before returning to a value close to the recess of the first pulse (near 2 mm). This behavior seems unlikely and further experiments are required to evaluate if this phenomenon is due to an artifact in the measurement or to fast plasma dynamics effects. These results indicate that the boundary of the cathode plasma (corresponding to the emission surface) changes with Δt, because the mechanisms of voltage increase and anode plasma formation have been excluded. Indeed, it was shown previously that a decrease of the recess induces an increase of the extracted current (see Fig. 5). Figure 8 illustrates the evolution of the plasma boundary, corresponding to the difference Δr between the recess at the first pulse and the recess at the second pulse, with Δt.

The current curves for different recess values built with the LSP model are used for all the experiments made with Mi2 to quantify the evolution of Δr with Δt. Figure 5 gives an example for $\Delta t = 2$ μs. Those curves link the extracted current with the emission surface position, i.e., the recess. Figure 9 presents the change in recess, Δr, of the plasma emission surface as a function of time delay Δt between the two pulses. Figure 9 includes the results presented in Fig. 7 and additional delays from other sets of experiments with an initial position of the velvet cathode estimated at 2.3 and 3.3 mm.

The overall trend shown in Fig. 9 suggests that Δr increases with Δt despite the large uncertainty in Δr values. The uncertainty is mainly due to the experimental measurement noise. Nevertheless, one can observe that the plasma effect on the emission surface position remains lower than 1 mm for 3 μs delay. In the literature, the plasma average expansion velocity $\langle v \rangle$ is estimated for the whole time of the pulse [18,19]. As the measurement of Δr is made between the middle of pulse plateaus, the average velocity may be defined as

$$\langle v \rangle = \frac{\Delta r}{\frac{\Delta t_{\text{plateau}_1}}{2} + \Delta t + \frac{\Delta t_{\text{plateau}_2}}{2}}.$$

It was previously mentioned that current measurements on pulse plateaus were noisy, preventing deduction of $\langle v \rangle$ for each pulse separately. A previous study realized on the first axis of EPURE with a current density similar to the experiments realized with Mi2 estimated an average velocity $\langle v \rangle = 0.53$ cm/μs [2]. Mi2 measurements of Δr as a function of Δt give a relatively slow velocity in the range of 0.025 cm/μs. If the average velocity was 0.53 cm/μs, then after 3 μs Δr should be 15.9 mm, a value 20 times larger than experimentally measured on Mi2. Starting from this statement, one can estimate that the emission surface expands at a reduced velocity between the two pulses of the Mi2 injector.

Considering the same recess evolution Δr as a function of the delay Δt obtained with the developed model and assuming that both pulses have the same voltage, Fig. 10 shows the ratio of the current extracted for the second pulse I_2 to the current extracted for the first pulse I_1 as a function of the delay between the pulses Δt. For $\Delta t < 500$ ns, Δr remains small, and the current produced at the second pulse remains close to the first pulse, i.e., $I_1 \approx I_2$. The plasma expansion between the two pulses induces only a current increase of 5% for the current extracted at the second pulse with a delay of 1 μs. For $\Delta t > 1$ μs, current ratios start to increase quickly which will complicate the electron beam transport in an accelerator. Although the use of velvet cathodes to produce two pulses in an injector induces an increase in the extracted current of the second pulse, results with $\Delta t < 500$ ns indicate that velvet cathodes may represent a potential candidate for multiple electron pulses.

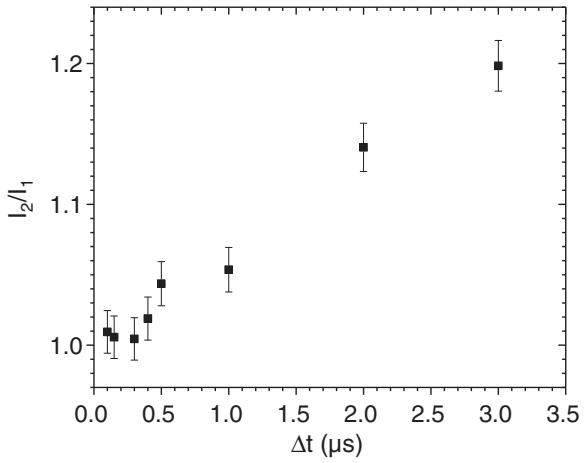

FIG. 10. Ratio of the current extracted for the second pulse I_2 to the current extracted for the first pulse I_1.

In addition, even if the mechanism of plasma expansion is not reproduced by the simulation, the current evolution as a function of the delay for velvet cathodes can be well reproduced with PIC modeling.

VI. CONCLUSION

Dual-pulse experiments were performed with the Mi2 injector to produce two 2 kA electron pulses from a velvet cathode. The current density of the experiments is representative of a multi-MV injector. Mi2 experimental results were realized to improve the comprehension and the modeling of the production of two intense electron pulses with a variable delay Δt between the pulses for flash radiography application. They were analyzed in order to measure the influence of Δt on the extracted current I_{ext} of the second pulse. Comparison of the experimental data with the simulation model developed for this dual-pulse study allows inferring the emission surface dynamics of the electron beam, and, hence, I_{ext}, with variable Δt. The model used in this study gives a good quantification of the extracted current variation for the beams produced. Results suggest that the emission surface position increases with Δt. This means that the emission surface moves away from a distance Δr of the velvet cathode even if there is an important uncertainty on its value. This uncertainty comes from the experimental measurement and also from the time chosen on the pulse plateau to build the curve $I_{\text{ext}} = f(r)$. Further experiments will be scheduled in order to improve experimental measurement and modeling. Nevertheless, the plasma effect on Δr is limited to 1 mm on 3 μs timescale. Results indicate that the emission surface expands at a reduced velocity in the dual-pulse regime on the Mi2 injector compared to the average velocity measured on EPURE axis-1. Furthermore, the model may be used to study other injector configurations with similar current density but with a higher voltage (>2 MV) representative of a multipulse LIA. Indeed, publications put forward that the plasma dynamics is governed by the average current density [15,18]. This assumption will be investigated in future experiments on the Mi2 injector to quantify the current density influence on plasma dynamics. This opens interesting perspectives in order to design and define the best strategy for an efficient multipulse machine based on the LIA technology. Finally, the impact on emittance, which was not discussed in this study, will also be the object of another study.

[1] K. Peach and C. Ekdahl, Particle beam radiography, Rev. Accel. Sci. Techol. **06**, 117 2013.
[2] J. M. Plewa *et al.*, High power electron diode for linear induction accelerator at a flash radiographic facility, Phys. Rev. Accel. Beams **21**, 070401 (2018).
[3] M. J. Burns *et al.*, Cell design for the DARHT linear induction accelerators, in *Conference Record of the 1991 IEEE Particle Accelerator Conference* (1991), Vol. 5, pp. 2958–2960, 10.1109/PAC.1991.165153.
[4] J. J. Deng *et al.*, Design of the DRAGON-I linear induction accelerator, in *Proceedings of the 21st International Linac Conference, Gyeongju, Korea* (2002).
[5] R. D. Scarpetti *et al.*, Upgrades to the LLNL flash X-ray induction linear accelerator (FXR), in *Digest of Technical Papers. 11th IEEE International Pulsed Power Conference (Cat. No.97CH36127)* (1997), Vol. 1, pp. 597–602, 10.1109/PPC.1997.679405.
[6] J. Deng *et al.*, Upgrading of linear induction accelerator x-ray facility (LIAXF), in *Proceedings of the 19th International Linear Accelerators Conference, Chicago, IL, 1998* (NTIS, Springfield, VA, 1998), pp. 389–390.
[7] M. Crawford and J. Barraza, Scorpius: The development of a new multi-pulse radiographic system, in *Proceedings of the 21st International Conference on Pulsed Power (PPC), Brighton, 2017* (2017), pp. 1–6, 10.1109/PPC.2017.8291266.
[8] M. Bizot *et al.*, Preliminary pusled power design of an induction injector for radiographic applications, in *2017 IEEE 21st International Conference on Pulsed Power (PPC)* (2017), pp. 1–6, 10.1109/PPC.2017.8291234.
[9] M. J. Burns *et al.*, Status of the DARHT phase 2 long-pulse accelerator, in *PACS2001. Proceedings of the 2001 Particle Accelerator Conference (Cat. No.01CH37268)* (2001), Vol. 1, pp. 325–329, 10.1109/PAC.2001.987505.
[10] J. Deng *et al.*, The Dragon-II, a triple pulse high power LIA, in *Proceedings of the 5th Eur-Asian Pulsed Power Conference, Kumamoto, Japan* (2014).
[11] D. A. Starostenko *et al.*, Status of the LIA-2. Double-pulse mode, Phys. Part. Nucl. Lett. **13**, 962 (2016).
[12] G. Westenskow *et al.*, Double pulse experiment with a velvet cathode on the ATA injector, in *Proceedings Particle Accelerator Conference* (1995), Vol. 2, pp. 1027–1029, 10.1109/PAC.1995.505118.
[13] M. Ong *et al.*, LLNL Flash X-ray Radiography Machine (FXR) Double-Pulse Upgrade Diagnostics, Report No. UCRL-JC-125879, 1997.

[14] Y. H. Wu and J. Ellsworth, Summary of beam operation capability at FXR LIA, in *Proceedings of the 9th International Particle Accelerator Conference, Vancouver, BC, 2018* (2018), pp. 3316–3319, 10.18429/JACoW-IPAC2018-THPAK045.
[15] L. Xia *et al.*, Investigations of the multi-pulsed emission characteristics of velvet, Appl. Surf. Sci. **251**, 262 (2005).
[16] R. B. Miller, Mechanism of explosive electron emission for dielectric fiber (velvet) cathodes, J. Appl. Phys. **84**, 3880 (1998).
[17] D. A. Shiffler *et al.*, Effects of anode materials on the performance of explosive field emission diodes, IEEE Trans. Plasma Sci. **30**, 1232 (2002).
[18] Y. E. Krasik *et al.*, Characterization of the plasma on dielectric fiber (velvet) cathodes, J. Appl. Phys. **98**, 093308 (2005).
[19] J. E. Coleman *et al.*, Explosive emission and gap closure from a relativistic electron beam diode, in *Proceedings of the 19th IEEE Pulsed Power Conference (PPC)* (2013), pp. 1–6, 10.1109/PPC.2013.6627454.
[20] Xia Lian-Sheng *et al.*, Velvet's multi-pulsed emission and multi-pulsed electron beams, Chin. Phys. **14**, 1779 (2005).
[21] Xia Lian-Sheng *et al.*, Multi-pulsed intense electron beam emission from velvet, carbon fibers, carbon nano-tubes and dispenser cathodes, Chin. Phys. C **34**, 1733 (2010).
[22] L. Xia *et al.*, Note: Design and initial results of a multi-pulsed intense electron beam source, Rev. Sci. Instrum. **85**, 066108 (2014).
[23] M. Toury *et al.*, Two pulses tests with a single LTD cavity, in *Proceedings of the Euro-Asian Pulsed Power Conference and the International Conference on High-Power Particle Beams, Karlsruhe* (2012).
[24] CST STUDIO SUITE®, CST AG, Germany, http://www.cst.com.
[25] B. Cassany *et al.*, Status of a 220KV–60NS flat top double pulse generator, in *Proceedings of the IEEE Pulsed Power Conference (PPC)* (2015), pp. 1–4, 10.1109/PPC.2015.7296882.
[26] P. Anthouard *et al.*, AIRIX and PIVAIR accelerator status, in *Conference Record of the Twenty-Third International Power Modulator Symposium (Cat. No. 98CH36133)* (1998), pp. 80–83, 10.1109/MODSYM.1998.741196.
[27] C. D. Child, Discharge from Hot CaO, Phys. Rev. **32**, 492 (1911).
[28] I. Langmuir, The Effect of Space Charge and Residual Gases on Thermionic Currents in High Vacuum, Phys. Rev. **2**, 450 (1913).
[29] A. Roy *et al.*, Plasma expansion and fast gap closure in a high power electron beam diode, Phys. Plasmas **16**, 053103 (2009).
[30] Y. Lau, Simple Theory for the Two-Dimensional Child-Langmuir Law, Phys. Rev. Lett. **87**, 278301 (2001).
[31] F. Hegeler *et al.*, Reduction of edge emission in electron beam diodes, Phys. Plasmas **9**, 4309 (2002).
[32] LSP is a software product of Orbital ATK.
[33] J. Yang *et al.*, Time-and-space resolved comparison of plasma expansion velocities in high-power diodes with velvet cathodes, J. Appl. Phys. **113**, 043307 (2013).
[34] J. M. Plewa *et al.*, Modeling and experimental characterization of the plasma produced by a velvet cathode in a linear induction accelerator, Phys. Plasmas **25**, 083506 (2018).
[35] J. A. Halbleib *et al.*, ITS: The integrated TIGER series of electron/photon transport codes—Version 3.0, IEEE Trans. Nucl. Sci. **39**, 1025 (1992).
[36] C. Vermare *et al.*, Ion emission from solid surfaces induced by intense electron beam impact, Phys. Plasmas **10**, 277 (2003).
[37] C. Ekdahl, Axis-I diode simulations I: Standard 2-inch cathode, LANL Report No. LA-UR-11-00206, 2011.
[38] C. Ekdahl, Current control for Scorpius, LANL Report No. LA-UR-19-25424, 2019.